Colloids and Surfaces A: Physicochemical and Engineering Aspects 686 (2024) 133403

Contents lists available at ScienceDirect

Colloids and Surfaces A: Physicochemical and Engineering Aspects

journal homepage: www.elsevier.com/locate/colsurfa

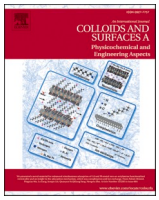

A small-angle X-ray scattering study of amphiphilic drug self-assemblies in polyacrylate microgels

Yassir Al-Tikriti, Per Hansson *

Department of Medicinal Chemistry, Uppsala University, Box 574, 75123 Uppsala, Sweden

GRAPHICAL ABSTRACT

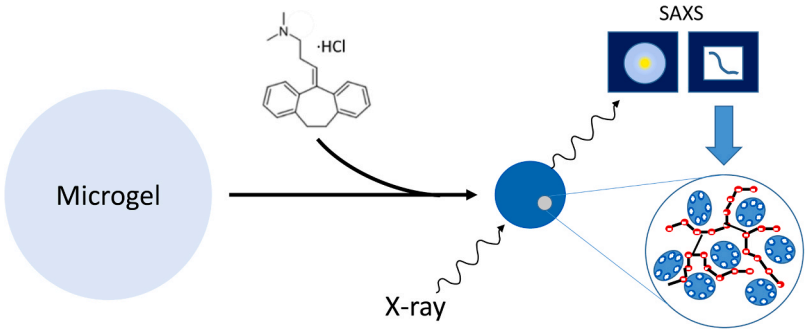

ARTICLE INFO

Keywords:
Amphiphilic drug
Microgel
Self-assembly
Small-angle X-ray scattering
Ellipsoidal packing
Polyelectrolyte

ABSTRACT

Common ionisable amphiphilic drug molecules form micelles in aqueous solution. Loaded onto oppositely charged polyelectrolyte microgels they associate with the network chains to form dense complex phases. The self-assembling properties control the loading and release properties in drug delivery applications of microgel systems but little is known about the nature of the aggregates and the phase structure. In this paper, we investigated the size and organization of the self-assemblies formed by the hydrochloride salts of amitriptyline (AMT), chlorpromazine (CPZ), and doxepin (DXP) in sodium polyacrylate microgels. Small-angle X-ray scattering (SAXS) was used to determine the microstructure of drug loaded microgels in aqueous environment at ionic strengths relevant for drug loading (0.01 M) and release (0.15 M). The composition of drug loaded microgels was determined by means of a purpose built microscopy cell and UV spectroscopy measurements. Upon drug loading the microgels formed complex phases of low water content. SAXS experiments showed that the drugs formed oblate shaped or spherical micelles displaying local ordering but without long-range ordering even at very high micelle volume fractions. The local ordering resembled the packing of randomly packed hard oblates and spheres. The aggregation number of AMT varied between 10 and 49 depending on the composition. Incorporation of the uncharged base form of the drug caused a transformation of oblate shaped (aspect ratio ~ 0.4) to spherical micelles, accompanied by an abrupt increase of the aggregation number. Variation of the ionic strength had minor effects on the aggregation number. CPZ formed oblate shape micelles (aspect ratios 0.3–0.4) with aggregation number between 9 and 30. DXP formed oblate shape micelles (aspect ratios 0.3–0.4) with aggregation numbers 10 – 11 at all studied compositions. The results provide a structural basis for, and justification of,

* Corresponding author.
E-mail address: per.hansson@ilk.uu.se (P. Hansson).

https://doi.org/10.1016/j.colsurfa.2024.133403
Received 5 December 2023; Received in revised form 17 January 2024; Accepted 3 February 2024
Available online 6 February 2024

previously assumed microstructures underlying mechanistic models of drug-microgel interactions and drug release.

1. Introduction

Cationic amphiphilic molecules are important active pharmaceutical substances that can be found in a wide range of pharmaceutical preparations, for example, anticancer drugs, antidepressants and antihypertensive agents [1,2]. The attraction between charged polymer microgels and oppositely charged amphiphilic molecules makes it possible to load large amounts of the drug inside the microgels, especially useful for labile or highly toxic substances [3,4]. For peptide and protein drugs, microgels offer protection against degradation, and the electrostatic interaction with the network makes it possible to control their release by elevating the ionic strength [5–9]. Furthermore, the pharmacological effect can be localized by applying the loaded microgels locally and triggering the release with the help of a triggering factor, such as ionic strength or pH [10,11]. One interesting drug delivery system is DC bead® which is licensed to treat liver cancer with doxorubicin as the active substance [12–15]. The beads contain a negatively charged polymer network, which upon loading with the oppositely charged doxorubicin forms a complex rich in drug aggregates. After intrahepatic administration to the blood vessels feeding the tumour, the beads swell upon the release of the drug. This causes embolization, which helps to decrease systemic spreading of the toxic drug. Ahnfelt et al. [16,17] studied the effect of the self-assembling properties on drug release from DC bead®. During the release, an aggregate-lean depletion layer (shell) formed in the outer layer of the gel that grew with time at the expense of the drug-rich core. They found that several other amphiphilic drugs behaved in a similar way, and that the release rate correlated with the critical micelle concentration (cmc) of the drug molecules. Based on that, they proposed that the drug release was rate controlled by the diffusive mass transport of drug molecules through the depletion layer. More precisely, the release rate was determined by the drug concentration gradient in the depletion layer, which under sink conditions depended on the thickness of the depletion layer and the concentration of drug monomers in the shell in local equilibrium with core.

In previous works [18,19], we have studied the interaction between amitriptyline hydrochloride (AMT) and highly responsive polyacrylate (PA) microgels. Under loading conditions at low ionic strength (10 mM), massive accumulation of drug aggregates inside the microgels took place for AMT concentrations in the solution exceeding the critical aggregation concentration (cac), which was ca. 100 times lower than the cmc in water. Loading was accompanied by a volume collapse of the microgel resulting in the formation of a highly concentrated complex phase. We studied the release of the drug in a medium of physiological ionic strength under sink conditions. Similar to DC bead®, we found that the process was governed by the internal depletion layer mechanism. In fact, we showed that the boundary between the depletion layer and the core was stabilized by thermodynamic factors, implying that during release the microgel underwent a phase transition. Such transitions, in the literature of gels referred to as a volume phase transitions (VPT) [20–23], take place between two competing states of similar free energy density, in the present case the collapsed complex phase and a drug-lean swollen phase. Considering that electrostatic interactions are effectively screened at physiological ionic strengths, the stability of the complex phase was somewhat unexpected. The result highlighted the importance of understanding the self-assembling properties of the drug molecules and the nature of the interaction between drug aggregates and the charged network, in order to be able to predict the drug release profile from microgel based delivery systems. However, structural information about drug self-assemblies in gels and the microstructure of drug-polyelectrolyte complex phases are very limited. To fill that gap, we investigate in this work the microstructure of PA microgels loaded with three amphiphilic drugs by means of small-angle X-ray scattering (SAXS). Our primary goal is to determine the organization of AMT in the microgels to provide structural information complementing our previous work. However, we investigate also the hydrochloride salts of two related drugs, chlorpromazine and doxepin, to explore how the introduction of substituents on the aromatic rings affects the self-assembling properties. Fig. 1 shows the chemical structures of the three molecules with their respective pK_a values indicated. The molecules possess the same polar head groups attached to a tricyclic hydrophobic moiety. Doxepin has an oxygen atom with a lone pair of electrons in the tricyclic hydrophobic system [24] while chlorpromazine has Cl, N and S substituents on the ring system.

2. Materials and methods

2.1. Materials

Amitriptyline hydrochloride (AMT) (≥ 98% TLC powder), chlorpromazine hydrochloride (CPZ) (≥ 98% TLC), doxepin hydrochloride (DXP) (~85% E-isomer basis, ≥98% (GC), 15% Z-isomer basis powder), sodium chloride, sodium phosphate monobasic (ReagentPlus® ≥ 99%), sodium phosphate dibasic (ReagentPlus® ≥ 99%) were from Sigma-Aldrich (St. Louis, MO, USA). Methanol (HPLC grade) was purchased from Fisher Chemical (Hampton, VA, USA). Sodium hydroxide was purchased from Riedel-de Haën (Sigma-Aldrich, St. Louis, MO, USA) and cyclohexane (≥ 99.5%) was purchased from Merk (Darmstadt, Germany). Acrylic acid (anhydrous 99%), N,N′-methylenebisacrylamide (99%), N,N,N′,N′-tetramethylethylenediamine (TEMED) (reagent plus 99%), ammonium persulfate (≥ 98%), and sorbitane monostearate (Span 60®) were from Sigma-Aldrich (St. Louis, MO, USA). All chemicals were used without further purification. Ultrapure (Type 1) water from Synergy® UV Water Purification System (Merck, Darmstadt, Germany) was used in all the preparations.

2.2. Microgels synthesis

Slightly cross-linked microgels were prepared by the inverse suspension polymerization technique following the procedure by Mayoux et al. with minor modifications, described in detail elsewhere [18,28]. In brief, the aqueous phase was obtained by mixing 2.6 g of acrylic acid, 109 μl of TEMED, 6.5 g of an 80 mM aqueous solution of the cross-linker N,N′–methylenebisacrylamide, 11 g of 2 M NaOH and water to a final volume of 20 ml. 0.09 g of Span 60 was dissolved in 30 ml of cyclohexane to form the organic phase. The organic phase was added to a two-necked round-bottomed flask under a nitrogen atmosphere and the temperature was set to 45 ℃. We then added 364 μl of 0.18 M ammonium persulfate to a 10 ml of the aqueous phase and injected it gradually into the organic phase while stirring at 400 rpm. The stirring rate was

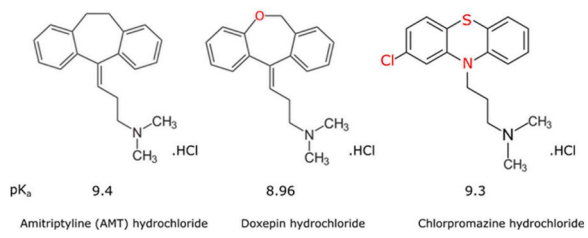

Fig. 1. The chemical structure of AMT, doxepin and chlorpromazine hydrochlorides. The pKa values, indicated in the figure from left to right, for AMT [25], doxepin [26] and chlorpromazine [27] respectively.

raised to 1000 rpm and the temperature set to 60 ℃. After 30 min, we stopped the reaction by adding 40 ml of methanol. Then the gel concentrate was removed and mixed with an excess of methanol. After removing the methanol phase, we dried the microgels at 60 ℃ in a Carbolite Furnaces airflow oven. Finally, the microgels were suspended in water, rinsed four times with water, and then stored in a refrigerator. The pH of the microgels suspension was kept at ~9.

2.3. Determination of swelling and binding isotherms

A technique described earlier [19] was used to determine the amount of drug inside single microgels. A single microgel was inserted in 1 ml of a drug solution by means of a micropipette. To avoid evaporation, the system was enclosed in a specially constructed cylindrical cell. The micropipette was prepared by using Narishige micropipette puller PN-31, micropipette grinder EG-400, and micro-forge MF-900 (Tokyo, Japan). The gel was equilibrated overnight and images were taken by using a Zeiss Axio Vert.A1 inverted microscope (Jena, Germany). The microscope was equipped with an AxioCam MRc camera, a Zeiss 10x/0.25 lens, and Narishige M-152 micromanipulator and Narishige IM-11–2 microinjector (Tokyo, Japan). After equilibration, the amount of drug bound to the microgel was determined in the following way. The gel was removed from the solution and inserted inside 250 μl of a 155 mM phosphate buffer to completely release the drug from the gel. The solution was collected and the concentration was measured by using a μDISS profiler from Pion Inc. (East Sussex, UK). The experiments were carried out at temperature 21 ± 1 °C. The amount of drug released was considered to be equal to the amount initially bound to the microgel. We corrected for the amount of drug absorbed to the wall of the container, as described elsewhere [19]. The molar concentration of the drug inside the gel was obtained by dividing the number of moles of the drug in the gel by the volume of the gel after equilibration. The binding ratio was calculated by dividing the number of moles of the drug in the gel by the number of moles of acrylate segments in the same gel. The latter was calculated from the volume of the microgel and the acrylate concentration inside microgels, as determined earlier [18].

2.4. Preparation of samples for SAXS

Samples were prepared by adding freeze-dried polyacrylate microgels to solutions of respectively amitriptyline, doxepin and chlorpromazine in 10 mM sodium phosphate buffer at pH 7.4, and equilibrated for at least two weeks at temperature 21 ± 1 °C. The amount of microgel was small to ensure that the concentration of drug in the solution did not decrease more than 2% from the initial value. In this way, we were able to determine the composition of the microgels by means of the swelling and binding isotherms determined in this study and elsewhere [18]. One set of samples was also prepared in solutions of higher ionic strength by equilibrating 4.4 mg freeze-dried PA microgels in 50 ml solution containing 3.4 mM AMT, 5 mM phosphate buffer, and 150 mM NaCl. According to binding data published elsewhere [19], this yields microgels with molar ratio 0.89 between drug and acrylate units.

2.5. Small-angle X-ray scattering (SAXS)

SAXS experiments were performed by using a Xeuss 2.0, Xenocs X-ray system equipped with a GeniX 3D microfocus X-ray source and Pilatus3 R 300 K detector operating without a beam stop. The distance between the sample and the detector was 270 mm. The gel samples were mounted between two Kapton films in a Xenocs vacuum-sealed gel holder. The exposure time was typically 3 h. The experiment was carried out at 22 °C in a temperature controlled room. The scattering from the buffer and the gel holder was subtracted from the raw data using the data reduction routine in the XSACT 2.4 software (Xenocs), a procedure correcting for measured transmissions and sample thickness. The intensities were displayed as a function of the scattering vector modulus $q = 4\pi\lambda^{-1}\sin(\frac{\theta}{2})$, where λ is the X-ray wavelength equal to 1.42 Å and 2θ is the scattering angle. The resulting data were analyzed by model fitting using the SasView 4.2.2 software. The scattering intensity $I(q)$ from the drug micelles in the gels was described with the form factor $P(q)$ for homogeneous spheres or core-shell ellipsoids of revolution. The model parameters describing the dimensions of the ellipsoidal core-shell micelles are the equatorial radius of the core (r_e), the polar-to-equator axial ratio of the core (X_c), the shell thickness at the equator (δ_e), and the ratio of shell thickness at the pole to that at the equator (X_p). From the fitted parameter values we calculated the ellipsoid's outer equatorial radius $a = r_e + \delta_e$, the outer polar radius $b = r_e X_c + \delta_e X_p$, and volume $V = 4\pi a^2 b/3$. The interaction between the micelles was described with the Hayter-Penfold structure factor $S(q)$ for charged spheres [29,30], taking into account the electric double layer repulsion between micelles by means of a screened coulomb potential. The structure factor includes as parameters the volume fraction of spheres, the charge of the sphere, the temperature, the concentration of salt, the dielectric constant of the medium, and the effective radius of the ellipsoids, calculated as the radius of a sphere with the same second virial coefficient as the ellipsoid. Only the first two were used as fitting parameters; the values of the last three were fixed and common for all fits. In all cases, 'background' and 'scale' were used as fitting parameters. The difference in scattering length density between the micellar core and the surrounding aqueous medium was kept fixed (-1.4 cm^{-1}). The scattering length density of the shell in the ellipsoidal micelles was used as a fitting parameter. It meant that the models for core-shell ellipsoids and homogeneous spheres contained, respectively, nine and five fitting parameters. Mathematical expressions of the form and structure factors are described in the SasView software and in, e.g., ref. [31].

3. Results and discussion

3.1. AMT-PA microgels

3.1.1. Binding and swelling isotherms for AMT-PA microgels

Fig. 2A shows the binding isotherm determined for the system AMT – PA microgel in buffered solutions (5 mM NaCl; 5 mM phosphate buffer; pH=7.4); C_{sol} is the AMT concentration in the solution in equilibrium with the microgel. We define the binding ratio β as the molar ratio of drug and polyacrylate monomer segments in the microgels. We have included, for reference, binding ratios below the range investigated here (open symbols), determined earlier [18]. Filled symbols are new measurements for samples with composition matching those used in the SAXS below. In all cases, the microgel underwent an AMT-induced volume collapse to a dense state. Fig. 3 shows microscopy images of the same microgels confirming that the collapsed microgels maintained the spherical shape of the swollen state prior to the collapse, and that they were homogeneous (i.e., monophasic). (The ring-shaped pattern visible on the microgels is characteristic of microscopy images of homogeneous spheres with refractive index different from that of the surrounding medium). Fig. 2B shows the microgel volume ratio as a function of C_{sol} for the same samples, where V is the actual volume and V_0 is the volume of the same microgel with $\beta = 0$.

From the binding and volume ratios we calculated the AMT concentration inside the microgels (C_{gel}), and from those values and AMT's molecular volume (493 Å^3) we calculated the corresponding AMT volume fraction (∅). Because the fraction of non-aggregated AMT in the microgels should be very small, we take ∅ to represent the volume fraction of micelles.

Table 1 shows the results from the binding and volume measurements for samples studied with SAXS. The binding ratio increased with increasing AMT concentration in the solution and reached values above unity. We expected this, because the driving force for binding from the hydrophobic effect alone should be strong enough to compensate for the entropic cost of co-binding negatively charged salt ions required to

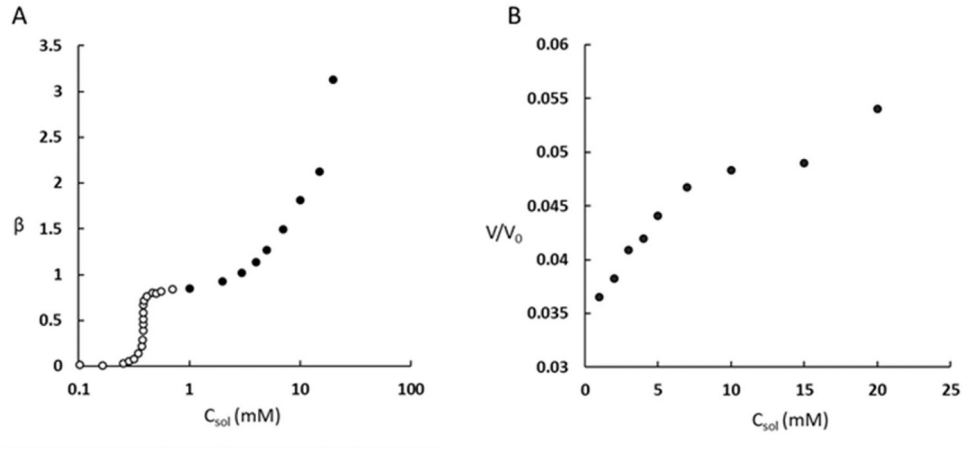

Fig. 2. Binding isotherm (A) and swelling isotherm (B) for the system AMT – PA microgel in buffered solution (5 mM NaCl; 5 mM phosphate buffer; pH=7.4). Open symbols were taken from ref. [18].

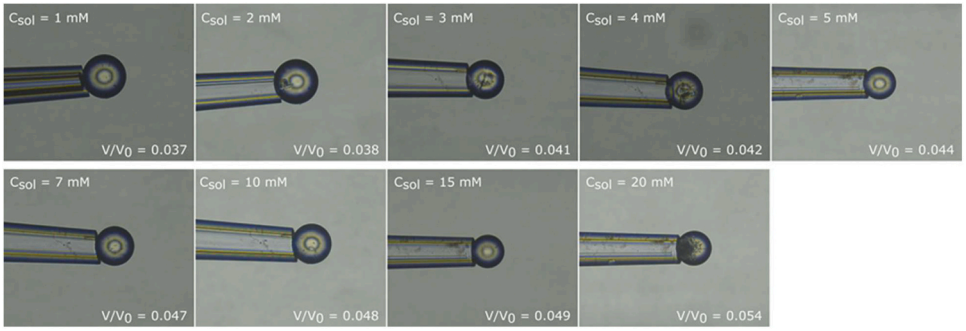

Fig. 3. Light microscopy images for polyacrylate microgels after 24 h equilibration in buffered solutions (5 mM NaCl; 5 mM phosphate buffer; pH=7.4) with different AMT concentrations (C_{sol}) as indicated. V/V_0 represents volume ratio where V represents the final volume after equilibration with AMT and V_0 represents gel volume in AMT-free state.

Table 1
Description of drug-PA microgel samples used in the SAXS study showing composition of the equilibrium drug solutions[a] (C_{sol}), the drug concentration in microgel (C_{gel}), binding ratio (β), microgel volume ratio (), drug volume fraction in gel, and calculated degree of dissociation of AMT (x). Temperature: 21 ± 1.

Drug	C_{sol}^{b} (mM)	C_{gel}^{c} (M)	β^{d}	V/V_0^{e}	$\varnothing^{f}$	x^{g}	β_{+}^{h}	$\varnothing_{SAXS}$	β_{est}
AMT	1	1.82	0.85	0.037	0.54	0.00	0.85	(0.68)	*0.85*
AMT	2	1.90	0.92	0.038	0.56	0.00	0.92	0.61	*0.92*
AMT	3	2.03	1.02	0.041	0.60	0.02	1.00	0.61	*1.02*
AMT	4	2.04	1.14	0.042	0.61	0.10	1.03	0.60	*1.14*
AMT	5	2.14	1.27	0.044	0.64	0.11	1.03	0.62	1.16
AMT	7	2.40	1.50	0.047	0.71	0.14	1.05	0.61	1.22
AMT	10	(2.8)	1.81	0.048	(0.84)	0.16	1.05	0.61	1.25
AMT	15	(3.5)	2.12	0.049	(1.0)	0.21	1.07	0.65	1.36
AMT	20	(4.3)	3.13	0.054	(1.3)	0.29	1.12	0.68	1.57
AMT[i]	2.6		0.89						
CPZ	0.25	2.63	1.23	0.035	(0.78)[j]				
CPZ	0.5	2.53	1.30	0.038	(0.75)[j]				
DXP	2	2.06	1.11	0.040	0.61				
DXP	5	2.04	1.13	0.040	0.61				

a) Buffered solutions (5 mM NaCl; 5 mM sodium phosphate buffer; pH=7.4)
b) Drug concentration in the solution in equilibrium with microgel
c) Drug concentration in the microgel
d) Molar ratio of drug and polyacrylate monomer segments in the microgel
e) Microgel volume relative to volume at $\beta = 0$
f) Drug volume fraction calculated from C_{gel} and AMT molecular volume of 493 Å^3
g) Calculated degree of dissociation of AMT in microgel
h) Calculated drug/polyacrylate charge ratio in microgel
i) 155 mM sodium phosphate buffer (pH=7.4)
j) Calculated assuming molecular volume 493 Å^3

maintain the microgels net electroneutral. However, we believe we have overestimated the three highest binding ratios since the volume fractions calculated from them are unrealistically high or physically impossible. We attribute that to a fraction of drug deposited as precipitates on the microgel surfaces, thereby not contributing to the concentration in the solution (cf. microgel at 20 mM AMT in Fig. 3). Because of that, we will hereafter use the accurately known value of C_{sol} to refer to a particular microgel system. However, it is important to keep in mind that C_{sol} is not at all representative of the drug concentrations *inside* the microgels, which is 2 - 3 orders of magnitude larger (Table 1). We will discuss the shape of binding and swelling isotherms as well as the quantities in Table 1 in more detail later.

3.1.2. SAXS results for AMT-PA microgels

Fig. 4 shows the scattering intensity as a function of the magnitude of the scattering vector q for PA microgels equilibrated in solutions of 1 – 20 mM AMT. At the three lowest concentrations, the scattering curves show a broad "correlation peak" at q≈0.3 $Å^{-1}$. At $C_{sol} \geq 4$ mM the curves develop a second broad peak with a maximum shifting to lower q with increasing β. Notably no Bragg peaks were observed, in contrast to what has been previously reported for a number of surfactant-polyelectrolyte gel systems at similar compositions [32–41]. The lack of long-range order shows that the microgels contained a solution of disordered micelles, corresponding to the L_1 phase in amphiphile – water systems. However, as will be demonstrated below, the structure factor strongly affects the scattering pattern, as expected for solutions of densely packed micelles. The effect is particularly large for samples with $C_{sol} \leq 7$ mM as shown by the suppressed scattering at low q. The curves for samples with $C_{sol} \geq 10$ mM are less affected by the structure factor and resemble those from concentrated AMT - water solutions recently published by Efthymiuo et al. [42]. The latter authors successfully fitted the SAXS curves with a model of oblate shaped, homogeneous spheroids, treating the effect of micelle-micelle interactions by means of the Hayter-Penfold structure factor for charged spheres [30,43].

Following Efthymiou et al., we analysed the SAXS curves in Fig. 4 with form factors for spheres and ellipsoids combined with the Hayter-Penfold structure factor. The data for the samples with $C_{sol} \leq 7$ mM could not be fitted with the form factors for homogeneous micelles, but core-shell models resulted in satisfactory fits. When we allowed the SasView software to simultaneously fit the equatorial and polar parameters, most cases resulted in oblate rather than prolate shaped ellipsoids. Furthermore, the prolate model completely failed to account for the scattering profile in the q range 0.4 – 0.6 $Å^{-1}$, where the oblate model performed well. When fitting the ellipsoidal model to the data for samples with $C_{sol} \geq 7$ mM, the equatorial and polar radii became practically identical and the shell thickness became very small, and the homogeneous spheres model gave good fits. From this we conclude that AMT formed oblate shaped micelles with core-shell structure for samples with $C_{sol} \leq 7$ mM and homogeneous spherical micelles for samples with $C_{sol} > 7$ mM. Fig. 5 shows the fits (thick solid curves) together with the experimental data (red crosses). Shown are also the form factor (dotted curve) and structure factor (thin solid curve) extracted out from the analysis in each case. The model describes the scattering curves well, except in the highest q-range. We attribute the upturn of the experimental curves in this range to a contribution from the polyacrylate chains.

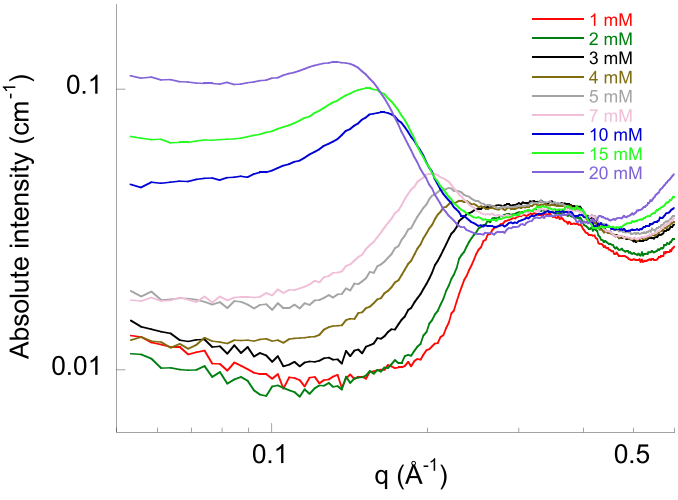

Fig. 4. SAXS data for polyacrylate microgels loaded with AMT in buffered solutions (5 mM NaCl; 5 mM phosphate buffer; pH=7.4). The legend shows the AMT concentration in the liquid solution (C_{sol}) in equilibrium with the microgels. Data recorded at 22 °C.

Table 2 shows the parameters determined from the fits, where a is the equatorial radius, b is the polar radius, δ is the shell thickness, V_{mic} is the micelle volume, N is the aggregation number and d_{S1} is the distance between neighbouring micelles. The latter was calculated from the relationship: $d_{S1} = 2\pi/q_{S1}$, where q_{S1} is the position of the first maximum of the structure factor. The micelle volume and the aggregation number were calculated using the relationships $V_{mic} = 4\pi a^2 b/3$ and $N = V_{mic}/V_{drug}$, where V_{drug} is the volume of the drug molecule, for which we used the value 493 $Å^3$ [42].

Fig. 6A shows how the equatorial diameter ($2a$), the polar diameter ($2b$), the shell thickness, the micelle-micelle separation, and the aggregation number vary as functions of C_{sol}. We first notice that d_{S1} nearly equals the largest dimension of the aggregates, showing that the micelles are almost in contact with their nearest neighbours at all compositions investigated. It agrees with our conclusion from binding and swelling isotherms that the volume fraction of micelles is very high in the microgels. A second thing to notice is that for $C_{sol} \leq 7$ mM there is a slight increase in the volume of the micelles at almost constant aspect ratio $\alpha\left(=\frac{b}{a}\right)$ (Table 2). However, a more dramatic increase takes place at C_{sol} between 7 and 10 mM, which is accompanied by a change of shape from oblate to spherical. In the narrow range where the shape transformation occurs, the polar diameter increases dramatically but the equatorial diameter remains essentially unchanged, showing that the micelles grow mainly along the direction of the polar semi-axis. For $C_{sol} \geq 10$ mM, the micelles are spherical but continue to increase in size with increasing amount of drug loading.

The oblate – sphere transition is accompanied by a minor jump in d_{S1} from a value slightly smaller than the largest oblate dimension to slightly larger than the sphere diameter, suggesting a change in the packing conditions. However, the microgel swelling and binding isotherms are continuous in that interval, indicating that the shape transformation is not accompanied by a 1st order phase transition. The micelle shell thickness δ decreases with increasing C_{sol}, and finally vanishes for $C_{sol} \geq 10$ mM, indicating a change in composition that we believe underlies the growth of the micelles, as will be discussed later.

To test the influence of salt we prepared one sample with $\beta = 0.89$ equilibrated in a solution with 155 mM sodium phosphate buffer (pH=7.4). Table 2 shows the results from the fit; for the SAXS curve and fit, see Supplementary Materials S1. A comparison with the results for the two lowest AMT concentrations at 10 mM sodium phosphate, having about the same binding ratio, shows that adding salt increases the aggregation number from 10 to 17. Furthermore, the influence of the structure factor decreases (Fig. S1). Both effects are in agreement with the expected effect of salt. Swelling isotherms determined earlier show that changing the conditions from $\beta = 0.84$/10 mM to $\beta = 0.89$/155 mM is accompanied by a slight increase of the gel volume, which is enough to decrease the AMT concentration in the gel. Similar effects have been observed in polyelectrolyte gel - surfactant systems [44]. For example, Nilsson et al. used SAXS to show that the micellar cubic phase formed by $C_{12}TA^+$ in PA gels swelled when salt was added and transformed into a disordered phase at sufficiently high salt concentrations

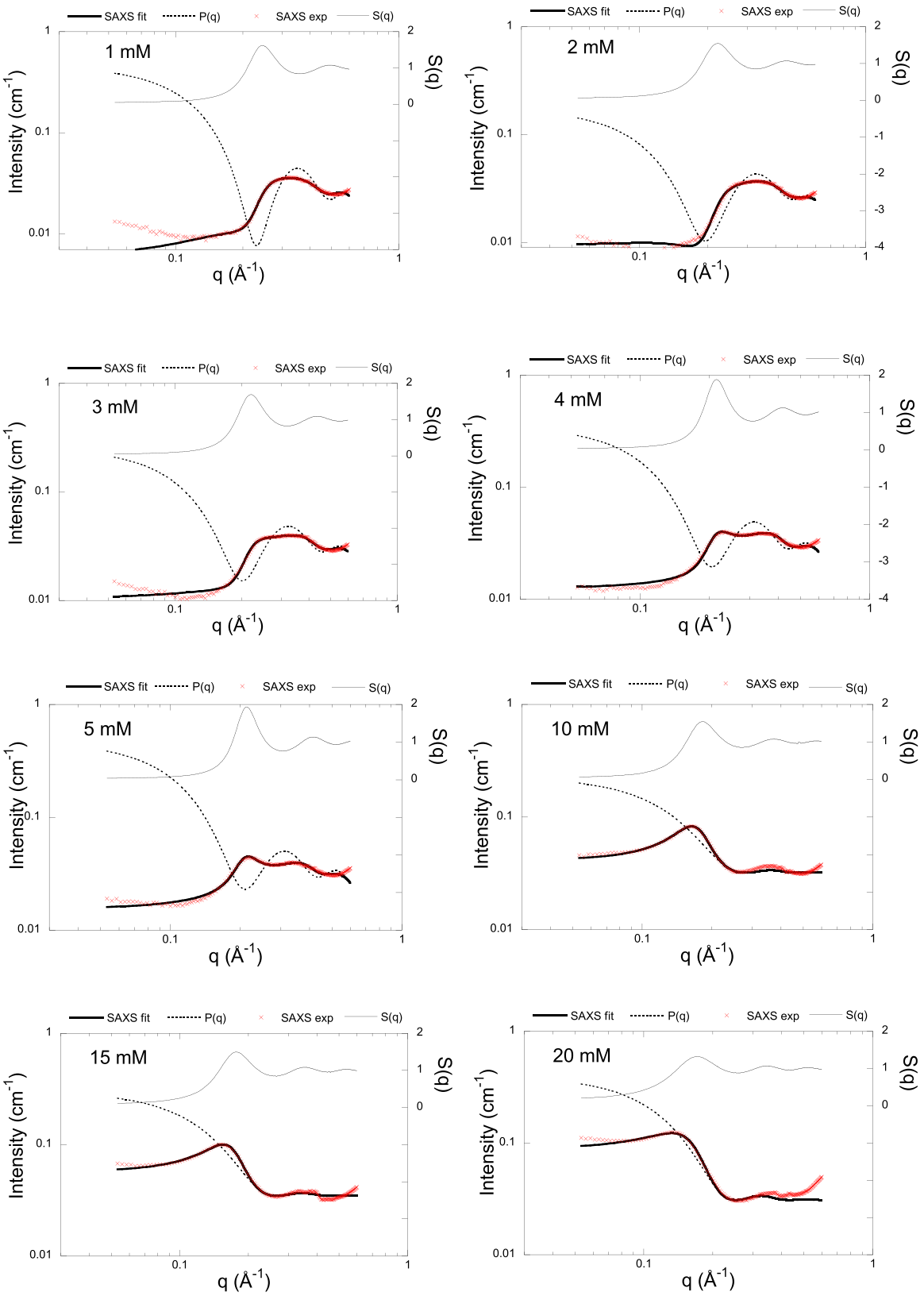

Fig. 5. SAXS intensity on absolute intensity scale plotted vs. q (red crosses) and results from model fitting (thick solid curves) for PA microgels equilibrated in AMT solutions with concentrations between 1 and 20 mM as indicated. Dotted curves: Determined form factor for core-shell oblate (1 – 5 mM) and homogeneous sphere (10 – 20 mM). Thin solid curves: Determined structure factor. Experimental data same as in Fig. 4.

Table 2
Size and shape characteristics of drug micelles determined from model fitting of the SAXS data recorded from complexes between PA microgels and AMT, CPZ and DXP, respectively, at temperature 22 °C.

Drug	C_{sol} (mM)	a (Å)[a]	b (Å)[b]	δ (Å)[c]	α[d]	V_{mic}^{e} (nm^3)	N[f]	d_{S1} (Å)[g]
AMT	1	14.3 ± 0.2	5.7 ± 0.3	1.7 ± 0.2	0.40	4.98 ± 0.41	9.9 ± 0.8	25.8
AMT	2	15.1 ± 0.0	5.7 ± 0.0	2.3 ± 0.0	0.37	5.39 ± 0.06	10.9 ± 0.1	28.3
AMT	3	15.2 ± 0.1	5.5 ± 0.0	1.9 ± 0.0	0.36	5.31 ± 0.07	10.8 ± 0.1	28.6
AMT	4	15.5 ± 0.1	5.8 ± 0.2	1.5 ± 0.1	0.37	5.82 ± 0.26	11.8 ± 0.5	29.2
AMT	5	15.8 ± 0.0	6.1 ± 0.0	1.3 ± 0.0	0.38	6.29 ± 0.02	12.8 ± 0.0	29.4
AMT	7	16.1 ± 0.0	6.7 ± 0.00	0.6 ± 0.0	0.41	7.26 ± 0.01	14.7 ± 0.0	30.2
AMT	10	16.1 ± 0.0	16.1 ± 0.0		1	17.5 ± 0.10	35.5 ± 0.2	34.3
AMT	15	17.0 ± 0.0	17.0 ± 0.0		1	20.7 ± 0.05	42.0 ± 0.1	35.5
AMT	20	17.9 ± 0.0	17.9 ± 0.0		1	23.9 ± 0.09	48.6 ± 0.1	36.7
AMT[h]		16.5 ± 0.1	7.1 ± 0.0	2.9 ± 0.0	0.43	8.16 ± 0.09	16.6 ± 0.2	29.5
CPZ	0.25	14.3 ± 0.6	6.1 ± 0.4	3.0 ± 0.5	0.43	5.22 ± 0.76	10.6 ± 1.5	26.2
CPZ	0.5	14.3 ± 0.2	4.8 ± 0.1	2.2 ± 0.2	0.33	4.09 ± 0.20	8.3 ± 0.4	27.3
CPZ	1	17.5 ± 0.0	6.1 ± 0.0	1.7 ± 0.0	0.35	7.80 ± 0.05	15.8 ± 0.1	29.9
CPZ	2	18.6 ± 0.1	7.3 ± 0.0	1.6 ± 0.0	0.39	10.6 ± 0.09	21.6 ± 0.2	33.2
CPZ	3	20.4 ± 0.1	8.6 ± 0.0	1.2 ± 0.0	0.42	14.9 ± 0.15	30.1 ± 0.3	34.9
DXP	2	14.1 ± 0.0	6.6 ± 0.0	1.0 ± 0.0	0.47	5.47 ± 0.09	11.1 ± 0.0	24.9
DXP	3	13.9 ± 0.0	6.6 ± 0.0	0.9 ± 0.0	0.47	5.32 ± 0.06	10.8 ± 0.1	24.8
DXP	4	14.1 ± 0.0	6.4 ± 0.0	0.5 ± 0.0	0.45	5.29 ± 0.05	10.7 ± 0.1	25.8
DXP	5	13.9 ± 0.0	6.1 ± 0.0	0.4 ± 0.0	0.44	4.95 ± 0.01	10.0 ± 0.0	25.2

a) Equatorial semi-axis radius (oblate spheroid)
b) Polar semi-axis (oblate spheroid)
c) Shell thickness
d) b/a
e) Micelle volume ($4\pi a^2 b/3$)
f) Aggregation number ($V_{mic}/493\text{Å}^3$)
g) Micelle-micelle separation ($2\pi/q_1$)
h) β= 0.89; 155 mM sodium phosphate buffer (pH=7.4)

(ca. 150 mM) [45]. Thus, we interpret the swelling as an effect of salt to weaken the interaction between micelles and the polyelectrolyte.

3.2. CPZ-PA microgels

3.2.1. Binding and swelling isotherms for CPZ-PA microgels

PA microgels equilibrated in CPZ solutions with concentrations 0.25, 0.5, 1, 2, and 3 mM were investigated by means of binding and swelling isotherms as well as by SAXS. Fig. 7 shows microscopy images of the microgels after equilibration for 24 h. At the two lowest concentrations, the microgels underwent a CPZ-induced volume collapse. Like with AMT, the microgels appeared homogeneous and maintained a spherical shape. However, in 1 – 3 mM CPZ solutions, they had attained non-spherical shapes and CPZ precipitates were deposited on the surfaces. Because of that, we only report binding and swelling ratios for the samples with 0.25 and 0.5 mM in Table 2.

3.2.2. SAXS results for CPZ-PA microgels

Fig. 8 shows the scattering curves from PA microgels loaded with CPZ. The scattering is somewhat stronger than from the AMT-PA samples, which we attribute the presence of the electron dense substituents S and Cl on the aromatic ring (cf. Fig. 1). Like for AMT, the scattering is markedly suppressed in the lower q-range, indicative of strong micelle – micelle interactions. The resulting correlation peak shifts to lower q with increasing concentration showing that the characteristic distance between micelles increases. Because the volume fraction of drug is very high, we interpret this as caused by the growth of close packed micelles. This is borne out by the results from model fittings exemplified by the curves for the samples with 0.25 and 3 mM CPZ in Fig. 9 (plots for the other samples are shown in S1). We were able to fit the oblate core-shell form factor combined with the Hayter-Penfold structure factor to all data sets, except in the low-q range where there is a an upturn in the scattering curves, most pronounced for the samples with the highest CPZ concentrations. The scattering in that range is indicative of large structures, possibly related to the precipitates on the microgels in those samples. Table 2 and Fig. 6B show the fitted parameters. N increases from ca. 10 to 30 in the studied range. The values are of the same order magnitude as determined for CPZ in water (N = 21) by small-angle neutron scattering measurements [46]. They are comparable also to those for AMT in the microgels but increases faster with increasing concentration in the solution. We believe the latter effect is because of the increased concentration of CPZ inside the microgel with increasing concentration in the solution, as shown by the data in Table 1. The aspect ratios are about the same as for the AMT oblate micelles, but change little with N. Hence, the CPZ micelles do not undergo oblate – sphere transition in the investigated range. However, as for the AMT oblate micelles, the characteristic distance d_{S1} between neighbouring micelles is even smaller than the equatorial diameter, showing that the micelles are almost in contact with their nearest neighbours.

3.3. DXP-PA microgels

Fig. 10 shows the scattering curve for PA microgels loaded with DXP. As shown by the solid curve the scattering from the microgel equilibrated in the solution with 2 mM DXP could be fitted with the oblate core-shell model. The resulting aggregation number is 11 and α = 0.41 (Table 2). The SAXS curves do not change much when the doxepin concentration in the solution increase from 2 to 5 mM, indicating that the dimensions of the micelles is almost constant (Fig. 6B). This is in agreement with the fact that the drug concentration in the gel is nearly constant in that interval (Table 1).

3.4. Why no Bragg peaks?

Systems of monodisperse hard spheres transform from disordered liquids to crystals at a volume fraction of ca. 0.5. The volume fractions for AMT in Table 1 are all larger than that, even approaching the close packing limit for spheres in FCC crystals (0.74). The majority of

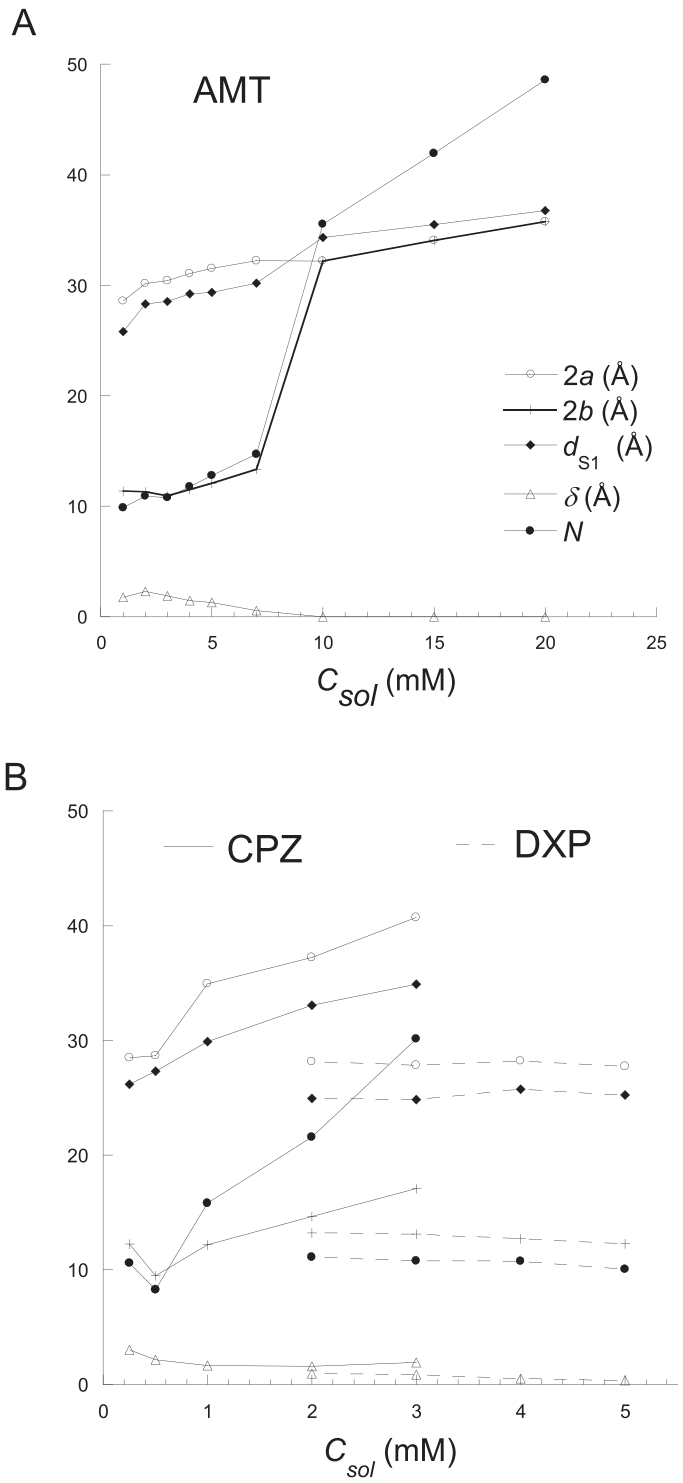

Fig. 6. SAXS results. **A**: AMT-PA; **B**: CPZ-PA and DXP-PA. Micelle equatorial diameter ($2a$), polar diameter ($2b$), shell thickness (δ), 1st correlation peak position (d_{S1}), and aggregation number (N) plotted vs. drug concentration in the liquid solution (C_{sol}). Symbols have the same meaning in **A** and **B**.

surfactant – gel systems described in the literature display ordered microstructures at compositions comparable to those of the present systems [32–41,47–49]. For example, $C_{12}TA^+$ forms a micellar cubic phase in PA gels ($\beta = 0.94$) already at a volume fraction of 0.37 [33,45]. In the light of that, it is remarkable that the present drug-gel systems maintain a disordered phase structure. We pointed out above that the volume fractions put in parentheses in Table 1 are unrealistic or physically impossible due to precipitation. However, we consider β and V/V_0 determined at the lowest C_{sol} to be reliable because they are in agreement with the results for AMT-PA macrogel systems, for which the determination of the quantities was straightforward [18]. Also for those gel compositions, any realistic estimate of the molecular volume of AMT gives volume fractions of 0.5. We will argue that the shape of the micelles and/or the comparatively small aggregation number and hence small micelle charge explain the lack of long-range order. We examine first the shape argument.

Quite recently, several research groups have investigated the packing conditions of hard ellipsoids. The results show [50] that hard oblates with aspect ratios $1/3 < \alpha < 1$ have a higher maximum packing volume fraction than hard spheres. For hard oblates with $\alpha = 0.4$, which is representative of the value for the oblate micelles formed here, the equilibrium transition from disordered to crystal takes place at volume fraction of ca. 0.6 [51]; the volume fraction in an ordered phase can be as high as 0.77 [52]. Hence, if our micelles behave as hard oblates they are very near the disordered-ordered phase boundary. Likewise, randomly close packed oblates can reach larger volume fractions than randomly close packed spheres. For example, oblates can reach volume fractions as high as 0.71 (simulations, $\alpha = 0.67$) and 0.69 (experiments, $\alpha \approx 0.5$) at random packing [53], as compared with a volume fraction of 0.64 for randomly close packed spheres [54]. For hard oblates with $\alpha = 0.4$ the corresponding value is ~0.68 [53,55], showing that the volume fraction of oblate micelles in our microgels (Table 1) are compatible with a disordered phase structure. Thus, there is evidence that hard ellipsoids can pack more efficiently than hard spheres in both the disordered and ordered states. We believe that is one reason why the phase structure in our microgels is lacking long-range order.

3.5. Local structure model

Results in the literature show that the way the volume fraction of randomly packed ellipsoids vary with the aspect ratio is similar to that of the equilibrium liquid-crystal phase boundary [50,51,53,55]. For instance, in both cases, the curve of the volume fraction as function of aspect ratio has a local maximum at aspect ratio ca. 0.6 and minimum at aspect ratio 1 (spheres), the main difference being that the curve for the liquid-crystal phase boundary is positioned at higher volume fractions than that for random close packing. It suggests that the local ordering in a disordered phase near the liquid-crystal phase boundary should resemble the phase structure in the crystalline phase. In fact, that principle has been used by others to rationalize relationships determined between scattering correlation peak position and volume fraction of micelles in SAXS and SANS studies of surfactant solutions [56].

Donev et al. [52] constructed a family of dense crystal packings with a unit cell containing two ellipsoids building an infinitely repeated two-layer lamination. By positioning the ellipsoids centred on the lattice points in the (001) plane of a face-centred cubic lattice of spheres, they obtained structures with higher packing volume fractions than for spheres. The highest volume fraction ($\varnothing_{max} = 0.770732$) was obtained for $\alpha = 1/\sqrt{3} \approx 0.58$ (oblates) in an arrangement where each ellipsoid touched six in-plane neighbours. For oblates with larger α, the packing density decreased with increasing α down to the value for fcc packing of spheres ($\pi/\sqrt{18} \approx 0.7405$). For $\alpha < 1/\sqrt{3}$ the volume fraction decreased rapidly with decreasingα. However, it was demonstrated that the maximum packing density could be achieved also for those aspect ratios by introducing an affine stretch along one direction of the (001) plane. We will now pursue the idea that the average separation between neighbouring ellipsoid in a disordered phase is approximately equal to the distance between ellipsoids in a crystalline phase uniformly swollen to the same volume fraction as the disordered phase. We start with the ordered structure proposed by Donev et al. and let the lattice expand uniformly by an arbitrary amount relative to the close packed state. Fig. 11 shows a "top view" and a "side view" of the structure, where L is

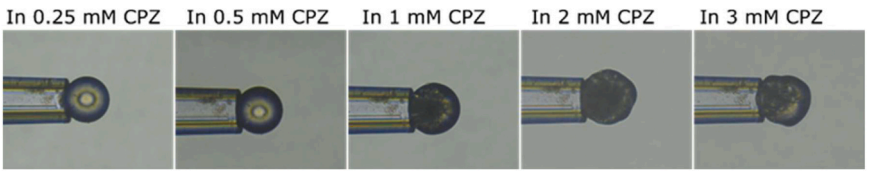

Fig. 7. Light microscopy images for polyacrylate microgels after 24 h equilibration with in buffered solutions (5 mM NaCl; 5 mM phosphate buffer; pH=7.4) with different chlorpromazine concentrations as indicated.

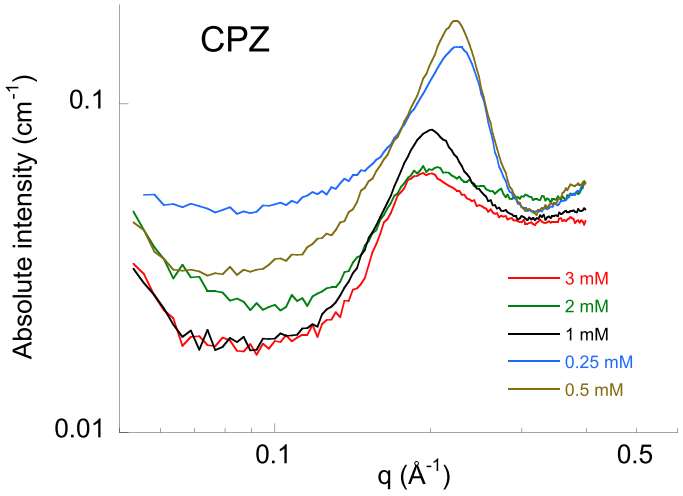

Fig. 8. SAXS data for CPZ-PA microgel. Legends show the chlorpromazine concentration in the solution in equilibrium with the microgels. The solutions were buffered (5 mM NaCl; 5 mM phosphate buffer; pH=7.4).

the length of the side of the layer based on the face-centred square lattice, h is the distance between two equally oriented layers, and $\overline{d}_1$, $\overline{d}_2$, and $\overline{d}_3$ are distances between neighbouring oblates; all quantities are expressed in units of a. Geometry gives $\overline{d}_1 = L/\sqrt{2}$, $\overline{d}_2 = \sqrt{L^2+h^2}/2$, and $\overline{d}_3 = L$. In the close packed state $L = L_{\min} = 2$and $h = h_{\min} = 4\pi/(\varnothing_{\max}\sqrt{27}) \approx 3.138$. For isotropic swelling we have: $\varnothing/\varnothing_{\max} = (L_{\min}/L)^3 = (h_{\min}/h)^3$.

Next, we show that results from computer simulations support the idea that local structural order in the disordered phase resembles the swollen crystalline lattice. Zhou et al. [55] used a discrete element method to simulate the packing of ellipsoidal particles formed under so-called poured packing. They found that oblates with $\alpha = 0.4$ gained a packing density of 0.66. Fig. 12A shows the radial distribution function (RDF) they obtained, where the scale on the abscissa shows the radial distance r in units of the oblate polar diameter ($2b$). The RDF reveals two important things. First, it lacks a maximum at $r/2b = 1$, in agreement with the Donev crystal structure. Second, instead of pair correlation peaks, the RDF has a broad "plateau" at $r/2b$ between 1.7 and 2.5, a range bounded quite accurately by the distances $\overline{d}_1$ and $\overline{d}_3$ in the swollen ordered structure in Fig. 11. This can be seen by expressing the distances on the scale used in Fig. 12A:

$$\frac{d_1}{2b} = \frac{d_1}{2\alpha a} = \frac{\overline{d}_1}{2\alpha} = \frac{L_{\min}}{2\alpha\sqrt{2}} = \frac{2}{2\alpha\sqrt{2}} = \frac{1}{\alpha\sqrt{2}} = \frac{1}{0.4 \bullet \sqrt{2}} \approx 1.8$$

$$\frac{d_2}{2b} = \frac{\sqrt{L_{\min}^2 + h_{\min}^2}}{2 \bullet 2b} = \frac{\sqrt{4a^2 + (3.138a)^2}}{2 \bullet 2b} = \frac{\sqrt{\alpha^2 + 2.462/\alpha^2}}{2} \approx 2.0$$

$$\frac{d_3}{2b} = \frac{\overline{d}_3}{2\alpha} = \frac{L_{\min}}{2\alpha} = \frac{2}{2\alpha} = \frac{1}{\alpha} = \frac{1}{0.4} = 2.5$$

Fig. 12B shows the structure factor for oblates (α=0.4; b=6 Å)

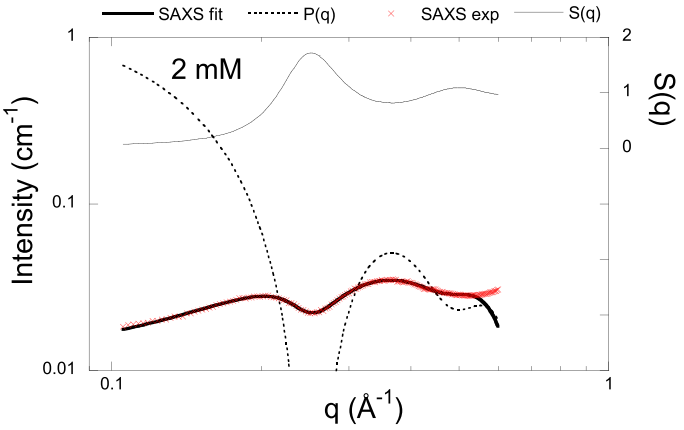

Fig. 10. SAXS data for DXP-PA microgel. Scattered intensity on absolute intensity scale plotted vs. q (red crosses) and results from model fitting (thick solid curves) for microgels equilibrated in 2 mM DXP solutions. Dotted curves: Determined form factor for core-shell oblate. Thin solid curves: Determined structure factor.

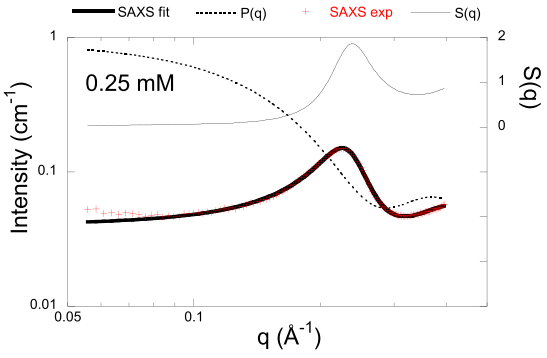

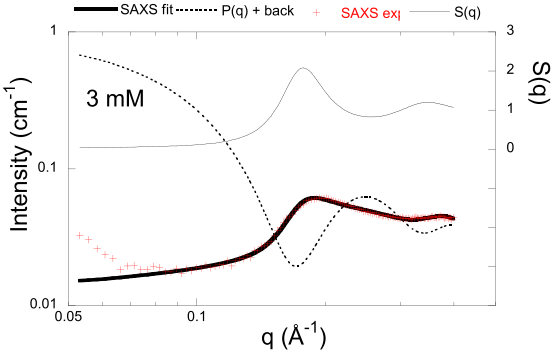

Fig. 9. SAXS intensity on absolute intensity scale plotted vs. q (red crosses) and results from model fitting (thick solid curves) for PA microgels equilibrated in CPZ solutions with concentration 0.25 and 3 mM as indicated. Dotted curves: Determined form factor for core-shell oblate. Thin solid curves: Determined structure factor.

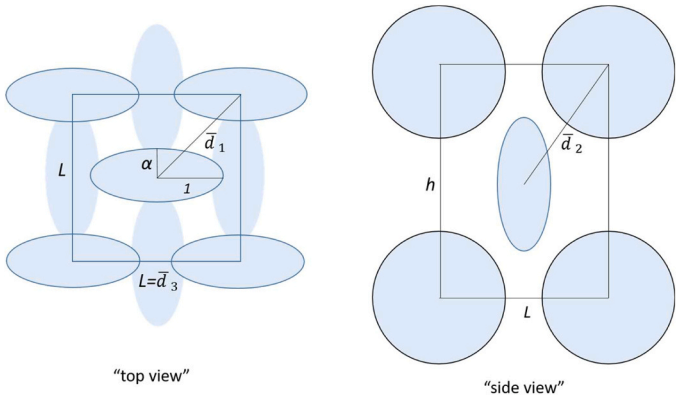

Fig. 11. Ordered packing of oblates placed on an isotopically swollen lattice constructed from two planar face-centred square layers rotated π/2 relative each other. Distances expressed in units of *a* (equatorial semi-axis). L is the length of the side of the layer.

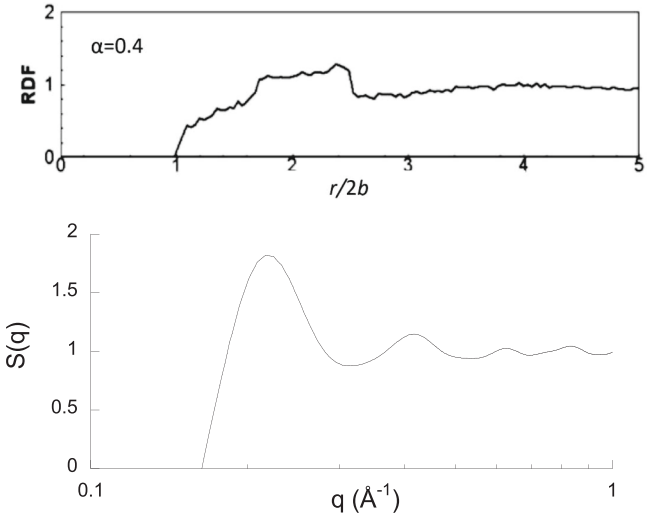

Fig. 12. Radial distribution function (RDF) for oblates ($\alpha = 0.4$; $\varnothing = 0.66$) adapted from computer simulation data by Zhou et al. [55], and structure factor S(q) calculated from the RDF for an oblate with b= 6 Å, $\alpha = 0.4$.

calculated from the RDF in Fig. 12A (see S2 for details). The result shows that despite the peculiar shape of the RDF, the structure factor's general appearance resembles the Hayter-Penfold structure factor for systems of charged spheres applied in our SAXS analysis. The first maximum is located at q= 0.3 Å^{-1}. This corresponds to a characteristic distance of 21 Å, which is intermediate between 2*b* and 2*a*. We conclude that disordered packing of oblates gives rise to local ordering with characteristic distance between neighbouring oblates similar to those in the ordered phase, and that the structure factor is expected to give rise to a correlation peak in SAXS at a *q*-value corresponding to characteristic distance *d*: $2b < d < 2a$.

3.6. Oblate – sphere transition in AMT-PA

For randomly close packed spheres (α =1) the RDF has a maximum at $r/2b = 1$ [55], i.e., the same as at maximum close packing of spheres (fcc lattice). Our SAXS results (Fig. 6A) indicate that the oblate – sphere transition is accompanied by a shift in the position of the first maximum in the structure factor, so that d_{S1}(sphere)/d_{S1}(oblate) = 1.14 (assuming a transition point at C_{sol}=8.5 mM). However, while there is a jump in the polar diameter (2*b*), the equatorial diameter (2*a*) is continuous through the transition point. Now, recall that there is no sign of discontinuities in the swelling and binding isotherms in the region where the shape transformation takes place. This indicates that the transition occurs at constant volume fraction of micelles. We can use this to derive swellings laws for the oblate and sphere regimes. For spheres on a swollen fcc lattice, with four micelles per unit cell of volume $2^{3/2}d^3$, where *d* is the nearest neighbour distance, the volume fraction is:

$$\varnothing_{\text{sphere}} = \frac{4 \bullet 4\pi}{3 \bullet 2^{3/2}} \left(\frac{r_{mic}}{d}\right)^3 \approx 5.92 \left(\frac{r_{mic}}{d}\right)^3 \quad (1)$$

Here, r_{mic} is the radius of a spherical micelle. With a=r_{mic} and volume fraction conserved at the transition, we obtain for the oblates:

$$\varnothing_{\text{oblate}} = 5.92 \left(\frac{d_{S1}(\text{oblate})}{d_{S1}(\text{sphere})}\right)^3 \left(\frac{a}{d}\right)^3 = \frac{5.92}{(1.14)^3} \left(\frac{a}{d}\right)^3 \approx 4.0 \left(\frac{a}{d}\right)^3 \quad (2)$$

Eqs. (1) and (2) provide a means to calculate the volume fraction of micelles from SAXS data, which is independent and complementary to the values calculated from the binding and swelling isotherms. The result is shown in Table 1. In Fig. 13, we compare the values with those obtained from the binding and swelling isotherms in Fig. 2. In the range C_{sol}< 7 mM, where we have no reason to question the accuracy of the data in Fig. 2, the two estimates values are in quite good agreement. The exception is at C_{sol}= 1 mM, where we believe the value calculated from SAXS is overestimated, perhaps because the micelles are packed differently. However, the estimates diverge for C_{sol}> 7 mM. In this range, the SAXS-based values are physically realistic and essentially compatible with a disordered phase structure, while the highest values calculated from the data in Fig. 2 are physically impossible. We cannot exclude that there could be a built-in systematic error in the SAXS determinations deriving from Eqs. (1) – (2), but we consider them to be quite accurate based on the good agreement with the determinations from the binding and swelling data in the lower concentration range. With that as a justification, we have calculated the binding ratio from the volume fractions determined with SAXS by means of the following equation:

$$\beta = \frac{V}{V_0} \bullet \varnothing_{SAXS} \bullet \frac{\bar{v}_0}{\bar{v}_{AMT}} \quad (3)$$

where $\bar{v}_0$ is the gel volume per moles of acrylate units in the microgel network in the swollen state (1.3 ×10^{-2} m^3/mole) and $\bar{v}_{AMT}$ is AMT's molar volume (2.97 ×10^{-4} m^3/mole). In the calculations, we used the volume ratio V/V_0 from the swelling isotherm (Table 1). The result, included in Fig. 13, shows that the binding ratio increases more moderately than in the binding isotherm in Fig. 2A, but reaches values well above unity at the highest concentrations. Again, the value for the

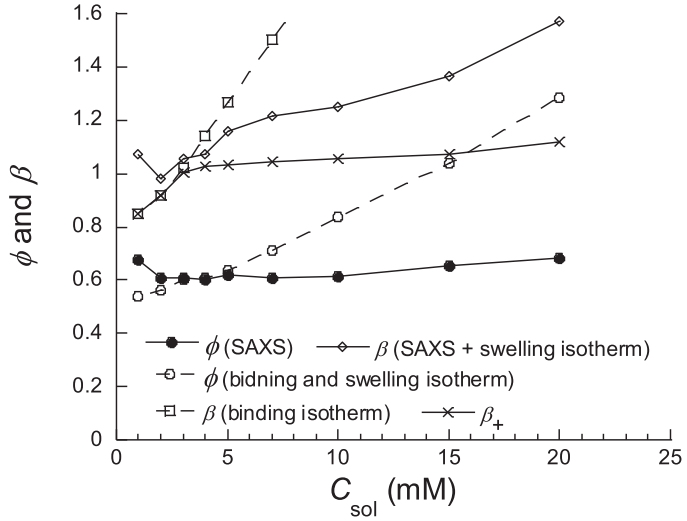

Fig. 13. Comparison of binding ratio (β) and volume fraction ($\varnothing$) determined from binding + swelling data and SAXS data in the AMT-PA microgel system.

lowest concentration deviates from the general pattern, suggesting that Eq. (2) is not applicable to that sample.

3.7. Charge regulation

An important question is why the gels continue to incorporate AMT into the already very dense structures to reach binding ratios well above unity. For common surfactants with permanent charge, binding ratios well above unity have been reported for oppositely charged gels in equilibrium with solutions at high ionic strength [47]. In contrast, at low ionic strength binding typically starts to level off at binding ratio close to unity because the entropic driving force from releasing network counterions is removed [57,58]. Nevertheless, even at low ionic strength, binding slowly increases with increasing concentration in the solution because the hydrophobic effect driving micelle formation and the coulomb interaction with the network charges continue to promote binding. However, increasing the binding ratios to values above unity comes with the entropy cost of co-binding surfactant counterions (e.g., Cl^-) which is substantial at low ionic strengths [58–60]. The fact that the binding ratio greatly exceeds unity in the present system is therefore quite remarkable. However, recall that the ionized "head group" of the AMT molecule consists of a protonated dimethylamine group that can donate the proton and become uncharged (pK_a= 9.4). Our theory is that, by recruiting the uncharged base form of AMT from the solution, the microgels can incorporate more drug molecules ($\beta > 1$) and at the same time avoid co-binding of counterions. To demonstrate that such an effect is realistic we have calculated the degree of dissociation (x) of AMT in the gel from the experimentally determined gel compositions, the electrolyte concentration in the solution, the pH of the solution and the pK_a of AMT. We have taken into account the electric potential difference between the gel and the solution by means of a Donnan equilibrium (see S3). The result, shown in Table 1, suggests that AMT is essentially fully ionized for $\beta < 1$, but when β exceeds unity the fraction of the uncharged form rapidly increases. The corresponding ratio of ionized AMT to network charges (β_+) (Table 1) levels out at a value slightly above unity, as shown in Fig. 13. Thus, the calculation suggests that mixed micelles form in the gels at the higher binding ratios. Further support comes from the observation that the SAXS-estimated thickness of the shell of the micelles decreased with increasing drug concentration inside the gel (Table 2). This indicates that the scattering from the head group region, including bound counterions, changes in such a way that the contrast between the core and the shell in the model decreases. We attribute that to an increasing fraction of deprotonated drug molecules in the micelles. In a recent SAXS study of AMT self-assemblies in pure water, Efthymiuo et al. [42] showed that the aggregation number increased from 34 near the CMC to 42 at 20 wt% (0.65 M), but then decreased down to 35 at 40 wt% (1.3 M). They attributed the non-monotonous variation to the combined effect of increasing the AMT concentration and the accompanying reduction of the pH, the latter effect changing the proportion of the protonated and deprotonated forms in the micelles. (Recall that the hydrochloride salt of the drug is a weak acid.) We conclude that, in order to continue incorporating drug molecules into the microgel at binding ratios > 1, the system regulates the charge of the micelles by recruiting the uncharged base form from the solution.

3.8. Micelle growth mechanism

The polar radius ($b+\delta$) of the oblate shaped micelles in the microgels (Table 2) is comparable in length to the maximum length of an AMT molecule (~8 Å; Fig. 1). Thus, the micelles appear to satisfy the condition that one dimension must remain smaller than or equal to twice the maximum length of the amphiphile [61]. Deprotonation should remove this constraint because the uncharged form needs not be anchored in the head group region of the micelle, thus making it possible for the micelles to increase their volume by undergoing a transition from oblate to sphere. However, since there is also the common effect that the spontaneous curvature decreases when a non-ionic amphiphile is incorporated into a charge aggregate, it remains to explain why the micelles grow by increasing the polar radius instead of increasing the equatorial radius. One may speculate that a spherical shape allows the amphiphilic monolayer to have a curvature more close to the preferred curvature than in a oblate shaped micelle (with small polar radius), e.g., by allowing the average surface area per molecule in the surface region to be smaller. Another factor is that decreasing the aspect ratio to values below 0.4 (here increasing the equatorial radius) should cause a larger reduction of the free volume per micelle than an increase of the aspect ratio to ca. 0.8 (increasing the polar radius). This can be inferred from simulations showing how the aspect ratio influences the volume fraction of randomly close packed oblates (see above).

Another notable feature is that the aggregation numbers in the lower β range are considerably smaller than for AMT in aqueous solutions, in spite of the fact that AMT is present in the microgels at higher concentration than in the solutions. The difference may reflect a difference between polyacrylate and chloride ions in their possibility to screen the repulsion between the AMT head groups. In contrast, for the microgels with the highest binding ratios, where chloride ions have been incorporated, the shape of the SAXS curves are similar to the ones for AMT (×HCl) solutions recorded by Efthymiuo et al. [42], and the aggregation numbers are of the same order of magnitude. In both solutions and microgels the smallest radius of the micelle is larger than the length ("head-to-tail") of the drug molecule, indicating that the micelles are swollen by uncharged drug molecules dissolved in the nonpolar core. This supports our argument that the incorporation of uncharged AMT in the micelles causes the oblate – sphere transition. The micelles in the solution differ from those in the microgels by being oblate shaped in the entire concentration range. However, in the solutions with the highest pH values, where the uncharged fraction is expected to be largest, the aspect ratio is ca. 0.8, meaning that the shape is almost spherical as in the microgels at the highest binding ratios. Interestingly, in both microgel and solution the aspect ratio increases with increasing fraction of the uncharged form in the mixed micelles (here we assume that the calculated fractions in the microgel are qualitatively correct and that in the solution the uncharged fraction increases with increasing pH). Thus, although the evolution of the aggregation number depends also on the AMT concentration, the aspect ratio appears to be more directly determined by the fraction uncharged drug molecules in the micelles.

3.9. Interaction between micelles

In the SAXS curves from AMT solutions [42], the maximum of the "correlation peak" shifts to higher q with increasing concentration, as explained by a decreasing separation between the micelles. In the microgels, where the micelles are close-packed at all investigated compositions, the maximum instead shifts to lower q with increasing concentration. The largest shift takes place at the oblate - sphere transformation where the growth of the micelles forces the distance between the centres of mass of neighbouring micelles to increase. Clearly, it is important to have a good description of the short-range interaction between the micelles. Lacking other options, we handled the interaction by means of the structure factor derived by Hayter-Penfold for charged spherical colloids within the rescaled mean spherical approximation. The model has been shown to be useful in the analysis of concentrated micellar systems, even under conditions where the screened coulomb potential is not valid [42]. In such cases, the parameters obtained from the fits describing the volume fraction and charge number of the micelles are less reliable or even unrealistic. This is the reason why we have not reported those parameters in Table 2. Because we apply the structure factor to model systems it was not designed to handle, it is important to discuss how relevant it is for the interactions encountered here. In the present system, the micelles attract each other with polyion-mediated forces, as indicated by the spontaneous enrichment of the drug in one part of the microgels at low binding

ratios, shown elsewhere [18,19]. However, in the very dense phases formed under such conditions, repulsions due to the confinement of the polyion-dressed micelles balance the attraction between the micelles. At short separations between micelles this is expected to give rise to electric double layer repulsions similar to the ones between micelles surrounded by small counterions [23,62]. Support of that view is provided by SAXS data showing that dodecyltrimethylammonium ions ($C_{12}TA^+$) in PA gels [35,45] (and in complexes with linear PA [63]) form a micellar cubic phase with the same space group (Pm3n) as C_{12}TACl in water [64] and C_{12}TAAc in water [63] when compared at the same water content (Cl=chloride; Ac= acetate). A screened coulomb potential is clearly not identical to the short-range interaction potential between polyion-dressed micelles, but should have a similar soft character. The form of the Hayter-Penfold structure factor is thus expected work as a reasonably good approximation to the structure factor for the spherical micelles in the present work. It is more difficult to motivate, a priori, the application of the Hayter-Penfold model to the oblate micelles. However, the shape similarity with the structure factor calculated from the radial distribution function for the disordered assembly of close packed oblates in Fig. 12, provides some justification.

The efficient packing of oblates can partly explain the absence of long-range order in the oblate micelle regime (see above). We believe that the small aggregation number is another contributing factor because the low charge of such micelles would to give rise to weak short-range repulsions. In the spherical micelle regime, where the micelles are comparatively large, the argument is slightly different. Here, we believe that deprotonation of the "head groups" decreases the short-range repulsion, leading to a shift of the disorder-order transition to higher volume fractions than expected for fully charge spherical micelles. In agreement with that explanation, Ashbaugh and Lindman [35] showed that the micellar cubic phase formed by $C_{12}TA^+$ in PA gels "melted" upon incorporation of the non-ionic surfactant $C_{12}E_8$ to form a disordered micellar phase. By means of SAXS measurements, they showed that a broad correlation peak replaced the distinct Bragg peaks characteristic of the Pm3n phase group. It is likely that, in our system, regulation of the micelle charge density by way of deprotonation of AMT has the effect of extending the stability range of the disordered phase to higher volume fractions, similar to that of incorporating a non-ionic surfactant.

4. Conclusion

We have investigated the microstructure of PA microgels loaded with respectively AMT, CPZ, and DXP with SAXS. In all studied samples, the loading level was large enough to transform the microgels to homogeneous complex phases of low water content. The drugs formed micelles in the microgels displaying local ordering but no long range ordering (no Bragg peaks), thus, formally, the phase structure should be denoted L_1.

The shape of the AMT micelles transformed from oblate to spherical in a narrow composition range. The oblates had equatorial radius of 15 $\pm$ 1 and polar radius of ca. 6 Å (axial ratio: 0.4) and aggregation number between 10 and 15, which is smaller than in aqueous solutions of AMT. The spherical micelles had radius of 17 $\pm$ 1 and aggregation numbers between 35 and 49, similar to aqueous solutions of AMT. Most likely, the recruitment of the non-ionized base form of AMT induces the shape transition, starting at drug/network charge ratio close to unity. We propose the following mechanism explains the transition. At ratios below unity, where the mean electrostatic potential is negative and hydrogen ions are enriched in the microgels, AMT is fully ionized. The micelles are restricted to have one dimension smaller than or equal to the double length of the drug molecule, but may grow in the other two dimension to form oblates of other aggregate types depending on the optimal packing of the molecules. At charge ratios above unity, where the mean electrostatic potential is positive and hydrogen ions are depleted from the microgels, a fraction of AMT is deprotonated. The uncharged form can solubilize in the micelle core. This removes the dimensional restriction, and so spherical micelles with radius larger than the length of the molecule will form if favoured by curvature over other aggregate shapes.

The unexpected absence of phase structures with long-range order in the oblate micelle regime is attributed to the high packing efficiency of oblates and the weak repulsion between (small) micelles with low charge, allowing them to form disordered phases at higher volume fraction than spheres. In the spherical micelle regime, where a fraction of the molecules are uncharged, the argument is that the interaction potential is softer than for fully ionized micelles because of lower surface charge density.

Increasing the ionic strength in the solution from 0.01 to 0.15 M had minor effects on the AMT aggregation number.

CPZ formed oblate shaped micelles with equatorial radius of 14 Å, polar radius of 5 Å (axial ratio: 0.3), and aggregation number 23 at molar ratio 1.3. DXP formed oblate micelles with equatorial radius of 14 Å, polar radius of 6–7 Å (axial ratio: 0.4), and aggregation number 11 at molar ratio 1.1.

This work provides the first quantitative determination of the size, shape and spatial arrangement of charged drug micelles inside oppositely charged microgel networks fully loaded with the drugs. The result is of large conceptual importance since it provides the structural basis underlying the strong interaction between amphiphilic drugs and polyelectrolyte networks, as well as the internal depletion layer mechanism governing the drug release rate observed in many systems of drug-eluting beads, including the doxorubicin-eluting DCbead® system used in liver cancer therapy. In future work, the generality of the charge regulation mechanism proposed to promote high drug loadings and induce microstructural transitions should be investigated.

Funding

This work was supported by Vinnova (Dnr 2019-00048).

CRediT authorship contribution statement

Hansson Per: Writing – review & editing, Writing – original draft, Visualization, Validation, Supervision, Methodology, Investigation, Funding acquisition, Formal analysis, Data curation, Conceptualization. **Al-Tikriti Yassir:** Writing – review & editing, Writing – original draft, Visualization, Validation, Methodology, Investigation, Formal analysis, Data curation, Conceptualization.

Declaration of Competing Interest

The authors declare that they have no known competing financial interests or personal relationships that could have appeared to influence the work reported in this paper.

Data Availability

Data will be made available on request.

Acknowledgement

We thank Dr. Adrian Rennie and Dr. Johan Gråsjö for providing expertise and technical assistance in connection with the SAXS experiments, and Dr. Jonas Gernandt for help with calculation of the oblate S (q). We thank Dr. Christel Bergström's group for letting us use their MicroDISS equipment. This study is part of the science program of the Swedish Drug Delivery Center (SweDeliver).

Appendix A. Supporting information

Supplementary data associated with this article can be found in the online version at doi:10.1016/j.colsurfa.2024.133403.

References

[1] D. Attwood, The mode of association of amphiphilic drugs in aqueous solution, Adv. Colloid Interface Sci. 55 (1995) 271–303.
[2] S. Schreier, S.V.P. Malheiros, E. de Paula, Surface active drugs: Self-association and interaction with membranes and surfactants, Physicochem. Biol. Asp. Biochim. Biophys. Acta- Biomembr. 1508 (2000) 210–234.
[3] T.R. Hoare, D.S. Kohane, Hydrogels in drug delivery: progress and challenges, Polymer 49 (2008) 1993–2007.
[4] A.S. Mikhail, M. Mauda-Havakuk, A.H. Negussie, N. Hong, N.M. Hawken, C. J. Carlson, J.W. Owen, O. Franco-Mahecha, P.G. Wakim, A.L. Lewis, et al., Evaluation of immune-modulating drugs for use in drug-eluting microsphere transarterial embolization, Int. J. Pharm. 616 (2022) 121466.
[5] M.T.A. Ende, N.A. Peppas, Transport of ionizable drugs and proteins in crosslinked poly(acrylic acid) and poly(acrylic acid-co-2-hydroxyethyl methacrylate) hydrogels. I. Polymer characterization, *J. Appl. Polym. Sci.* 59 (1996) 673–685.
[6] H. Bysell, P. Hansson, M. Malmsten, Transport of poly-l-lysine into oppositely charged poly(acrylic acid) microgels and its effect on gel deswelling, J. Colloid Int. Sci. 323 (2008) 60–69.
[7] H. Bysell, M. Malmsten, Interactions between homopolypeptides and lightly cross-linked microgels, Langmuir 25 (2009) 522–528.
[8] G.M. Eichenbaum, P.F. Kiser, A.V. Dobrynin, S.A. Simon, D. Needham, Investigation of the swelling response and loading of ionic microgels with drugs and proteins: The dependence on cross-link density, *Macromolecules* 32 (1999) 4867–4878.
[9] M. Malmsten, H. Bysell, P. Hansson, Biomacromolecules in microgels - opportunities and challanges for drug delivery, Curr. Opin. Colloid Interface Sci. 15 (2010) 435–444.
[10] R. Narayanaswamy, V.P. Torchilin, Hydrogels and their applications in targeted drug delivery, Molecules 24 (2019) 603.
[11] N.A. Peppas, P. Bures, W. Leobandung, H. Ichikawa, Hydrogels in pharmaceutical formulations, Eur. J. Pharm. Biopharm. 50 (2000) 27–46.
[12] M. Dadsetan, Z. Liu, M. Pumberger, C.V. Giraldo, T. Ruesink, L. Lu, M.J. Yaszemski, A stimuli-responsive hydrogel for doxorubicin delivery, Biomaterials 31 (2010) 8051–8062.
[13] K. Fuchs, R. Duran, A. Denys, P.E. Bize, G. Borchard, O. Jordan, Drug-eluting embolic microspheres for local drug delivery - state of the art, J. Control. Release 262 (2017) 127–138.
[14] O. Jordan, A. Denys, T. De Baere, N. Boulens, E. Doelker, Comparative study of chemoembolization loadable beads: In vitro drug release and physical properties of dc bead and hepasphere loaded with doxorubicin and irinotecan, J. Vasc. Interv. Radio. 21 (2010) 1084–1090.
[15] A.L. Lewis, R.R. Holden, Dc bead embolic drug-eluting bead: clinical application in the locoregional treatment of tumours, Expert. Opin. Drug. Deliv. 8 (2011) 153–169.
[16] E. Ahnfelt, J. Gernandt, Y. Al-Tikriti, E. Sjögren, H. Lennernäs, P. Hansson, Single bead investigation of a clinical drug delivery system – a novel release mechanism, J. Control. Release 292 (2018) 235–247.
[17] E. Ahnfelt, E. Sjögren, P. Hansson, H. Lennernäs, In vitro release mechanisms of doxorubicin from a clinical bead drug-delivery system, J. Pharm. Sci. 105 (2016) 3387–3398.
[18] Y. Al-Tikriti, P. Hansson, Drug-eluting polyacrylate microgels: loading and release of amitriptyline, J. Phys. Chem. B 124 (2020) 2289–2304.
[19] Y. Al-Tikriti, P. Hansson, Drug-induced phase separation in polyelectrolyte microgels, *Gels* 8 (2022) 4.
[20] Y. Hirokawa, T. Tanaka, Volume phase transition in a non-ionic gel, J. Chem. Phys. 81 (1984) 6379–6380.
[21] S. Hirotsu, Critical points of the volume phase transition in n-isopropylacrylamide gels, J. Chem. Phys. 88 (1987) 427–431.
[22] K. Sekimoto, M. Doi, Dynamics of interface of gels undergoing volume phase transition, J. Phys. II Fr. 1 (1991) 1053–1066.
[23] P. Hansson, Volume transition and phase coexistence in polyelectrolyte gels interacting with amphiphiles and proteins, Gels 6 (2020) 24.
[24] P. Taboada, D. Attwood, J.M. Ruso, M. García, V. Mosquera, Static and dynamic light scattering study on the association of some antidepressants in aqueous electrolyte solutions, Phys. Chem. Chem. Phys. 2 (2000) 5175–5179.
[25] A.L. Green, Ionization constants and water solubilities of some aminoalkylphenothiazine tranquillizers and related compounds, J. Pharm. Pharm. 19 (1967) 10–16.
[26] K. Embil, G. Torosian, Solubility and ionization characteristics of doxepin and desmethyldoxepin, J. Pharm. Sci. 71 (1982) 191–193.
[27] I.J. AP, Limiting solubilities and ionization constants of sparingly soluble compounds: determination from aqueous potentiometric titration data only, Pharm. Res. 5 (1988) 772–775.
[28] C. Mayoux, J. Dandurand, A. Ricard, C. Lacabanne, Inverse suspension polymerization of sodium acrylate: Synthesis and characterization, J. Appl. Polym. Sci. 77 (2000) 2621–2630.
[29] J.-P. Hansen, J.B. Hayter, A rescaled msa structure factor for dilute charged colloidal dispersions, Mol. Phys. 46 (1982) 651–656.
[30] J.B. Hayter, J. Penfold, An analytic structure factor for macroion solutions, Mol. Phys. 42 (1981) 109–118.
[31] J.S. Pedersen, Analysis of small-angle scattering data from colloids and polymer solutions: modeling and least-squares fitting, Adv. Colloid Interface Sci. 70 (1997) 171–210.
[32] V.A. Kabanov, A.B. Zezin, V.B. Rogacheva, Y.V. Khandurina, Absorption of ionic amphiphils by oppositely charged polyelectrolytes, Macromol. Symp. 126 (1997) 79–94.
[33] P. Hansson, Surfactant self-assembly in polyelectrolyte gels: Aggregation numbers and their relation to the gel collapse and the appearance of ordered structures in the napa/c12tab system, Langmuir 14 (1998) 4059–4064.
[34] P. Hansson, S. Schneider, B. Lindman, Phase separation in polyelectrolyte gels interacting with surfactants of opposite charge, *J. Phys. Chem. B* 106 (2002) 9777–9793.
[35] H.S. Ashbaugh, B. Lindman, Swelling and structural changes of oppositely charged polyelectrolyte gel-mixed surfactant complexes, Macromolecules 34 (2001) 1522–1525.
[36] S. Zhou, C. Burger, F. Yeh, B. Chu, Charge density effect of polyelectrolyte chains on the nanostructures of polyelectrolyte-surfactant complexes, Macromolecules 31 (1998) 8157–8163.
[37] S. Zhou, F. Yeh, C. Burger, B. Chu, Nanostructures of polyelectrolyte gel-surfactant complexes, J. Polym. Sci.: Part B: Polym. Phys. 37 (1999) 2165–2172.
[38] B. Chu, F. Yeh, E.L. Sokolov, S.G. Starodoubtsev, A.R. Khokhlov, Interaction of slightly cross-linked gels of poly(diallyldimethylammonium chloride) with surfactants, Macromolecules 28 (1995) 8447–8449.
[39] E.L. Sokolov, F. Yeh, A. Khokhlov, B. Chu, Nanoscale supramolecular ordering in gel-surfactant complexes: sodium alkyl sulfates in poly(diallyldimethylammonium chloride), Langmuir 12 (1996) 6229–6234.
[40] F. Yeh, E.L. Sokolov, A.R. Khokhlov, B. Chu, Nanoscale supramolecular structures in the gels of poly(diallyldimethylammonium chloride) interacting with sodium dodecyl sulfate, J. Am. Chem. Soc. 118 (1996) 6615–6618.
[41] F. Yeh, E.L. Sokolov, T. Walter, B. Chu, Structure studies of poly (diallyldimethylammonium chloride-co-acrylamide) gels/sodium dodecyl sulfate complex, Langmuir 14 (1998) 4350–4358.
[42] C. Efthymiuo, L.M. Bergström, J. Nedergaard Pedersen, J.S. Pedersen, P. Hansson, Self-assembling properties of ionisable amphiphilic drugs in aqueous solution, J. Colloid Int. Sci. 600 (2021) 701–710.
[43] J.B. Hayter, J. Penfold, Determination of micelle structure and charge by neutron small-angle scattering, Colloid Polym. Sci. 261 (1983) 1022–1030.
[44] P. Hansson, Volume transition and phase coexistence in polyelectrolyte gels interacting with amphiphiles and proteins, Gels 6 (2020) 24.
[45] P. Nilsson, J. Unga, P. Hansson, Effect of salt and surfactant concentration on the structure of polyacrylate gel/surfactant complexes, *J. Phys. Chem. B* 111 (2007) 10959–10964.
[46] V. Perez-Villar, M.E. Vazquez-Iglesias, A. de Geyer, Small-angle neutron scattering studies of chlorpromazine micelles in aqueous solutions, J. Phys. Chem. 97 (1993) 5149–5154.
[47] A.V. Mironov, S.G. Starodubtsev, A.R. Khokhlov, A.T. Dembo, A.N. Yakunin, Ordered nonstoichiometric polymer gel-surfactant complexes in aqueous medium with high ionic strength, Macromolecules 13 (1998) 7698–7705.
[48] A.T. Dembo, A.N. Yakunin, V.S. Zaitsev, A.V. Mironov, S.G. Starodubtsev, A. R. Khokhlov, B. Chu, Regular microstructures in gel-surfactant complexes: influence of water content and comparison with the surfactant structure in water, *J. Polym. Sci.: Part B: Polym. Phys.* 34 (1996) 2893–2898.
[49] S. Sasaki, S. Koga, M. Sugiyama, M. Annaka, Nanostructures of polyelectrolyte gel-surfactant complexes in uniaxially stretched networks, Phys. Rev. E 68 (2003) 021504.
[50] A. Bezrukov, D. Stoyan, Simulation and statistical analysis of random packings of ellipsoids, Part. Part. Syst. Char. 23 (2006) 388–398.
[51] D. Frenkel, B.M. Mulder, The hard ellipsoid-of-revolution fluid, Mol. Phys. 55 (1985) 1171–1192.
[52] A. Donev, F.H. Stillinger, P.M. Chaikin, S. Torquato, Unusually dense crystal packings of ellipsoids, Phys. Rev. Lett. 92 (2004) 255506.
[53] A. Donev, I. Cisse, D. Sachs, E.A. Variano, F.H. Stillinger, R. Connelly, S. Torquato, P.M. Chaikin, Improving the density of jammed disordered packings using ellipsoids, Science 303 (2004) 990–993.
[54] G.D. Scott, D.M. Kilgour, The density of random close packing of spheres, J. Phys. D: Appl. Phys. 2 (1969) 863.
[55] Z.-Y. Zhou, R.-P. Zou, D. Pinson, A.-B. Yu, Dynamic simulation of the packing of ellipsoidal particles, Ind. Eng. Chem. Res. 50 (2011) 9787–9798.
[56] M. Ludwig, R. Geisler, S. Prévost, R. von Klitzing, Shape and structure formation of mixed nonionic–anionic surfactant micelles, Molecules 26 (2021) 4136.
[57] P. Hansson, Interaction between polyelectrolyte gels and surfactants of opposite charge, Curr. Opin. Colloid Interface Sci. 11 (2006) 351–362.
[58] P. Hansson, Surfactant self-assembly in oppositely charged polymer networks. Theory, J. Phys. Chem. B 113 (2009) 12903–12915.
[59] J. Gernandt, P. Hansson, Hysteresis in the surfactant-induced volume transition of hydrogels, J. Phys. Chem. B 119 (2015) 1717–1725.
[60] J. Gernandt, P. Hansson, Surfactant-induced core/shell phase equilibrium in hydrogels, J. Chem. Phys. 144 (2016) 064902.
[61] F. Evans, H. Wennerström, The colloidal domain: Where physics. chemistry, biology, and technology meet, VCH Publishers, New York, 1994.
[62] A. Svensson, L. Piculell, L. Karlsson, B. Cabane, B. Jönsson, Phase behavior of an ionic surfactant with mixed monovalent/polymeric counterions, J. Phys. Chem. B 107 (2003) 8119–8130.
[63] S. dos Santos, C. Gustavsson, C. Gudmundsson, P. Linse, L. Piculell, When do water-insoluble polyion-surfactant ion complex salts “redissolve” by added excess surfactant? Langmuir 27 (2011) 592–603.
[64] R.R. Balmbra, J.S. Clunie, J.F. Goodman, Cubic mesomorphic phases, Nature 222 (1969) 1159–1160.